DAF-2/insulin IGF-1 receptor regulates mobility during ageing

by integrating opposite inputs from muscle and neuronal tissues

Charline Roy[1], Laurent Molin[1], Mathilde Solyga[1], Benjamin Bonneau [1,2], Camille Vachon[1], Jean-Louis Bessereau[1,] Florence Solari[1*].

[1]Université de Lyon, Université Claude Bernard Lyon 1, CNRS UMR 5310, INSERM U 1217, Institut NeuroMyoGène, Lyon 69008, France; [2] Present address: Institut Curie, PSL Research University, Université Paris-Saclay, CNRS UMR 3347, INSERM U1021, Orsay 91405, France

Correspondence
Institut NeuroMyoGene, Laboratory of Genetics and Neurobiology of *C. elegans*, Université de Lyon, Université Claude Bernard Lyon 1, CNRS UMR 5310, INSERM U 1217, Faculté de Médecine et de Pharmacie, 3ème étage-Aile D 8, Avenue Rockefeller, Lyon 69008, France.
corresponding author* ***Email: florence.solari@univ-lyon1.fr*

Key words: *daf-2*, degron, mobility, lifespan, *daf-16*, oxidative stress, mitochondria, insulin/IGF1 signaling.

Short title: Regulation of mobility by DAF-2 in adulthood

SUMMARY

During ageing, preservation of locomotion is generally considered an indicator of sustained good health, in elderlies and in animal models. In *C. elegans,* mutants of the insulin receptor DAF-2 represent a paradigm of healthy ageing, as their increased lifespan is accompanied by a delay in age-related loss of mobility. However, these animals are less mobile than wild-type animals in early adulthood. Here we investigated the DAF-2-dependent relationship between longevity and mobility using an auxin-inducible degron to trigger tissue-specific degradation of endogenous DAF-2. As previously reported, inactivation of DAF-2 in neurons or intestine was sufficient to extend the lifespan of worms, whereas depletion in epidermis, germline or muscle was not. However, neither intestinal nor neuronal depletion of DAF-2 prevented the age-related loss of mobility. In 1-day-old adults, DAF-2 depletion in neurons reduced mobility, while muscle depletion had no effect. By contrast, DAF-2 depletion in the muscle of middle-age animals improved their mobility. The combination of neuronal and muscle effects thus mimics the global locomotor phenotype of *daf-2* mutants. Yet, we observed that neuronal or muscle DAF-2 depletion both preserved the mitochondria network in ageing muscle. Overall, these results show that the mobility pattern of *daf-2* mutants is determined by the sequential and opposing impact of neurons and muscle tissues and can be dissociated from the regulation of the lifespan. This work also provides the characterization of a versatile tool to analyze the tissue-specific contribution of insulin-like signaling in integrated phenotypes at the whole organism level.

INTRODUCTION

Ageing has long been regarded as an inevitable process resulting from a gradual and passive deterioration over time, as illustrated by the 'wear and tear' theory of ageing. However, genetic studies in the nematode *Caenorhabditis elegans* have revealed that a single mutation in the *daf-2* gene can double lifespan[1]. *Daf-2* encodes the sole ortholog of the mammalian insulin and IGF-1 receptors (IIR) and its role in regulating lifespan appears to be conserved in mammals [2]. *Daf-2* mutants were initially isolated for their constitutive formation of diapausal larvae, called dauer (Daf-c phenotype). The long-lived and Daf-c phenotypes of *daf-2* mutants require the FOXO transcription factor DAF-16 [3,4]. Activation of the DAF-2/IIR triggers a cascade of phosphorylation responsible for the retention of DAF-16/FOXO into the cytoplasm[5–8]. Downregulation of this pathway promotes DAF-16/FOXO accumulation into the nucleus where it activates hundreds of genes [9].

Decline in physical performance is a universal feature of ageing. *daf-2* mutants show improved movement ability in mid-adulthood that may be due to preserved motoneurons function [10,11]. Thus, *daf-2* mutants not only have a long lifespan, but are also considered healthier in old age. Yet, we and others [12] noticed that in early adulthood, *daf-2* mutants are less mobile as compared to wild-type animals. This observation questions the relationship between lifespan and the other phenotypic traits considered as markers of good health. One way to tackle this question is to identify the tissue(s) where DAF-2 inactivation is required to cause specific phenotypes and test to which extent long-life and other phenotype are linked.

To date, very little is known about the physiological expression pattern of DAF-2. An immunolabelling approach has shown that DAF-2 is expressed mainly in the nervous system and in a pair of cells called "XXX cells" in the head and also in the epidermis [13]. In addition, two studies analyzed the requirement of DAF-2 or DAF-16 in different tissues for lifespan regulation using transgene rescue of *daf-2 or daf-2; daf-16* mutants[14,15]. The first study concluded that DAF-2 acts primarily in the nervous system, consistent with the expression profile of DAF-2, while the second study concluded that DAF-16 acts principally in the gut. This was counter-intuitive because these two proteins function in the same signaling pathway. The paradox was resolved by proposing that intestinal DAF-16 may in fact trigger a secondary signal from the gut to induce inhibition of DAF-2 in distant neuronal tissues [15]. However, these studies relied on standard transgenesis strategies, the only tools available at that time, that lead to overexpression levels and miss some regulatory elements present in endogenous loci. In support of the model involving interorgan inactivation of the DAF-2 pathway, a more recent study reported that communication between neuronal DAF-16 and intestinal DAF-16 is responsible for extending the lifespan of *C. elegans* [16]. Yet, the DAF-16 analysis was also based on the use of an overexpressed DAF-16::GFP fusion protein that may not reflect the endogenous regulation of the DAF-16 protein. New

technologies have flourished to manipulate the endogenous expression of specific proteins, providing a way to re-examine the tissue-specific function of DAF-2, as we still do not know in which tissue DAF-2 is normally required for the regulation of the different phenotypes observed in *daf-2* mutants.

In this work, we investigated when and where DAF-2 is required to maintain worm mobility during adulthood and how this phenotype relates to the dauer, lifespan and oxidative stress resistance phenotypes. In order to deplete DAF-2 protein in a spatially and temporally controlled manner, we generated alleles for conditional degradation by inserting an auxin-inducible degron (AID) [17] and a fluorescent tag into the *daf-2* locus and constructed different strains to induce DAF-2 degradation in all cells or in neurons, muscle, intestine, germline or hypodermis. Our results show that DAF-2 is ubiquitously expressed in worms and can be efficiently degraded by the AID system. Degradation of DAF-2 in all tissues, from adulthood onwards, reproduced the lifespan and motility phenotypes of the reference *daf-2 (e1370)* allele and the constitutive dauer phenotype in the progeny. Depletion of DAF-2 in neurons or in the gut was sufficient to extend the lifespan of the worms but only intestinal inactivation of DAF-2 increased resistance to oxidative stress. However, intestinal inactivation did not improve worm mobility in adulthood. Furthermore, the mobility of worms in adulthood appeared to be controlled by a positive impact of DAF-2 activity in neurons, acting from early adulthood and an negative effect of DAF-2 activity in muscles from middle age. While muscle inactivation of DAF-2 improved the mobility of the worms, it did not affect their lifespan or their resistance to oxidative stress. Finally, our data show that inactivation of DAF-2 in muscle or neurons was sufficient to induce nuclear accumulation of DAF-16 in the same tissue but not in distant tissues, strongly suggesting that inter-organ inactivation of the DAF-2 pathway is not a prerequisite for regulation of mobility during ageing.

RESULTS

The AID:mNeonGreen-tagged DAF-2 protein is functional and efficiently degraded in the presence of auxin.

The mNeonGreen (mNG) and degron sequences were added to the 3' end (before the STOP codon) of the endogenous *daf-2* locus (*daf-2::AID::mNG or kr462*) so that DAF-2 degradation could be monitored via the loss of mNG fluorescence. DAF-2::AID::mNG was detected in head neurons, XXX cells and epidermis as previously reported but also in the majority of the worm tissues (**Figure 1a**). *Daf-2(kr462)* worms were crossed with two independent lines that expressed in all tissues the plant ubiquitin ligase substrate recognition subunit, TIR1, an essential component of the AID system, (see **Table S1** for strains description). We then verified that neither the tag nor the presence of the TIR1 transgene interfered with DAF-2 function. In the absence of auxin, *daf-2(kr462)* and *daf-2(kr462)*; *Pubiquitous*::TIR1 worms exhibited the same lifespan (**Figure 1b; c**, **Table S2**) and mobility (**Figure 1d; e)** as wild-type worms at

different temperatures. Furthermore, they did not enter the dauer stage at any temperature in the presence of food, in contrast to the heat-sensitive reference *daf-2(e1370)* mutants that showed a fully penetrant dauer constitutive phenotype (**Table S3**). Thus, the addition of the degron and mNG sequences to the *daf-2* locus or TIR1 ubiquitous expression did not impair DAF-2 function.

In the presence of auxin, the fluorescence signal was strongly downregulated after 24 hours, confirming the efficiency of auxin-induced DAF-2 degradation (**Figure 2).** We then assessed the dauer, lifespan and mobility phenotypes of *daf-2(kr462)* worms expressing TIR1 in all tissues compared to *daf-2(e1370)* mutants. All transgenic worms placed on auxin from hatching entered the dauer stage at 15, 20 or 25°C, (**Table S3** and data not shown), mimicking the fully penetrant dauer phenotype of *daf-2(e1370)* mutants raised at the restrictive temperature of 25°C. Furthermore, when *daf-2(kr462)* worms were placed on auxin plates at a later developmental stage (L4) to bypass the dauer arrest, their lifespan was doubled, as *daf-2(e1370)* worms at 20°C (**Figure 1c and Table S2**). Remarkably, the ubiquitous degradation of DAF-2 also recapitulates the age-dependent mobility phenotype of *daf-2(e1370)* mutants. Indeed, 1-day-old and 13-day-old *daf-2(kr462)* worms expressing TIR1 in all tissues showed a lower and higher frequency of body bends, respectively, compared to control animals of the same age (**Figure 1d; e**). Overall, these data demonstrate that the downregulation of DAF-2::AID::mNG correlates with a significant reduction of DAF-2 function, validating our experimental approach. However, the reference *daf-2(e1370)* allele is considered hypomorphic because predicted null *daf-2* mutations cause early developmental phenotypes with embryonic arrest[18]. This suggests that some functional DAF-2 protein remains during early development, in agreement with the persistent low level of embryonic fluorescence detected in the progeny of adults grown in the presence of auxin (**Figure 1e**). Nevertheless, our results show that inactivation of DAF-2 during development is not a prerequisite for lifespan extension, in agreement with previous results[19,20], and that down-regulation of DAF-2 in adulthood is also sufficient to recapitulate the effect of constitutive down-regulation of DAF-2 on worm mobility during ageing.

Intestinal and neuronal DAF-2 activities cooperate to regulate lifespan but are differently required for the resistance of worms to oxidative stress.

We first examined the tissue-specific contribution of DAF-2 inactivation to the regulation of dauer and lifespan. Transgenic lines were generated to express TIR1 in muscle (*Pmyo-3*), hypodermis (*Pdpy-17*), neurons (*Prab-3*), gut (*Pges-1*) or germline (*Psun-1*). In addition to the previously described TIR1 transgenes (**Table S1**), we generated new transgenes in order to test two independent lines for each tissue and thus limit potential confounding effect of the genetic background (see Experimental procedures). In the presence of auxin, these TIR1 transgenes effectively degraded the DAF-2::AID::mNG protein from individual tissues, as assessed by the loss of fluorescent signals in young

adult and middle aged animals after 24 hours (**Figure S1**). Dauer formation could not be achieved after degradation of DAF-2 in one given tissue (**Table S3**) thus suggesting that DAF-2 functions in several tissues and/or in other cells than the main tested tissues to control dauer entry. These observations are in contradiction with previous data showing that overexpression of *daf-16* in the nervous system of *daf-2; daf-16* double mutants recapitulated the Daf-c phenotype of *daf-2* mutants[15]. However, recent work on the tissue-specific activities of DAF-16 in a wild-type context argues that DAF-16 is required in several tissues to control the dauer phenotype [21], in agreement with our results with DAF-2.

Inactivation of DAF-2 in muscle, hypodermis or germline had no impact on lifespan (**Figure 3a-f**). Degradation of DAF-2 in neurons or intestine was sufficient to increase the median lifespan by 41% and 51%, respectively. However, none of these tissues recapitulated the lifespan increase caused by ubiquitous DAF-2 inactivation (**Figure 3a-k and Table S2**) in agreement with recent work from Venz et al.[20] .Combined DAF-2 degradation in both neurons and gut did not further extend the lifespan of animals as compared to worms with intestinal DAF-2 degradation alone. Thus, additional cells or a different combination of tissues may be involved in the regulation of lifespan by DAF-2.

Resistance to oxidative stress has been proposed as a mechanism responsible for the extension of lifespan by DAF-2[22]. In the presence of paraquat, a reactive oxygen species generator, ubiquitous or intestinal inactivation of DAF-2 consistently increased the lifespan of worms compared to control worms, although to a lesser extent for intestinal lines (**Figure 3l**). Neuronal inactivation of DAF-2 caused a slightly higher resistance to paraquat in one line, and a slightly lower resistance in the second one (**Figure 3m**), although both lines were long-lived in the absence of paraquat (**Figure 3i; j).** These results are similar to those obtained by Venz et al. [20]with different TIR1 strains. In addition, we showed that neuronal inactivation of DAF-2 reduced the resistance to oxidative stress of worms with intestinal DAF-2 depletion **(Figure 3n**), but this reduction was not associated to a shorten lifespan in absence of paraquat **(Figure 3k**). Therefore, intestinal degradation of DAF-2 is sufficient to confer both resistance to oxidative stress and prolonged lifespan, but these two phenotypes may be uncoupled. Resistance to oxidative stress is also not a prerequisite for the longevity phenotype that is induced by neuronal inactivation of DAF-2.

Overall these data strongly suggest that the regulation of lifespan by DAF-2 involves signaling from neuronal and intestinal tissues with some shared downstream mechanisms, as a similar extension of lifespan is achieved after inactivation of DAF-2 in one or both tissues, but also with distinct physiological consequences.

DAF-16 nuclear accumulation upon tissue-specific inactivation of DAF-2

Early studies on the tissue-specific activities of DAF-2 and DAF-16 have suggested that down-regulation of the DAF-2 signaling pathway in one tissue induces its inhibition in distant tissues[14,15]. However, these results were obtained in a sensitized genetic background, as all cells were mutant for *daf-2*. More recent data support this model in a *daf-2(+)* background by showing that activation of intestinal or neuronal DAF-16 induces nuclear accumulation of overexpressed DAF-16::GFP in distant tissues[16]. To avoid potential issues associated with reporter transgenes such as overexpression, we endogenously tagged DAF-16/FOXO with SCARLET using CRISPR/Cas-9 mediated genome engineering. DAF-16:: wrmSCARLET was detected in all somatic tissues and the germline during adulthood, with highest expression in neurons, and localized mainly in the cytoplasm of all cells **(Figure 4a)**. Ubiquitous depletion of DAF-2 from the L4 stage induced nuclear accumulation of DAF-16 in all tissues **(Figure 4b)** and the whole progeny entered the dauer stage (data not shown), confirming that the DAF-16:: wrmSCARLET protein was functional.

Tissue-specific degradation of DAF-2 in neurons or muscle from L4 onwards induced nuclear accumulation of DAF-16:: wrmSCARLET in the same tissue but not in distant tissues **(Figure 4d-e)**. However, depletion of DAF-2 in the intestine was associated with nuclear accumulation of DAF-16::wrmSCARLET in the gut and muscles, but not neurons. Hence, the longevity phenotype associated with DAF-2 inactivation in the gut might involve the inactivation of the DAF-2 pathway in distant tissues, but not in neurons. Furthermore, the extension of lifespan by neuronal depletion of DAF-2 does not seem to involve the intestinal inactivation of DAF-2. Thus, the shared mechanisms between the intestinal and neuronal activities of DAF-2 for lifespan regulation do not involve an inactivation of DAF-2 through inter-organ communication. Finally, neuronal and muscle DAF-2 activity in lifespan or mobility (see below) does not rely on DAF-2 inactivation in distant tissues.

DAF-2 neuronal signaling is required for worm mobility in early adulthood

In order to further characterize the fitness of long-lived worms we measured their body-bend frequency in liquid medium (BBF), as a proxy of physical performance [23]. Declined mobility of worms with age has been associated with both decreased neural stimulation and decline of muscle cell integrity [11,12,24]. The mobility of worms with DAF-2 inactivation in the intestine was similar to that of control worms on days 1 and 13 of adulthood (**Figure 5a).** Thus, the signaling from the intestine upon DAF-2 degradation is sufficient to prolong lifespan, but does not markedly affect the function of the neuromuscular system with age. Conversely, neuronal inactivation of DAF-2 significantly reduced BBF and mirrored the mobility of worms with whole body degradation of DAF-2 in 1-day-old animals **(Figure 5a).** This observation is rather unexpected as a previous study proposed that the *daf-2(e1370)* mutation maintains neurosecretion of motor neurons compared to wild-type worms [11]. Our

observations suggest instead that neuronal DAF-2 depletion inhibits neuronal stimulation of muscle contraction. Worms mobility requires alternating contractions of antagonist muscles that is achieved through a network involving excitatory cholinergic and inhibitory GABAergic motoneurons. To further test our hypothesis, we induced DAF-2 degradation specifically in excitatory or inhibitory neurons. Depletion of DAF-2 in GABAergic neurons did not significantly affect worm's mobility while its inactivation in cholinergic neurons downregulated worm's mobility similarly to worms with pan-neuronal inactivation of DAF-2 in 1-day-old animals **(Figure 5b)**. These data suggest that in wild-type animals, neuronal DAF-2 controls muscle activity in early adulthood through activation of the cholinergic neural network. Furthermore, the role of DAF-2 in neuronal excitatory signaling may also be involved in lifespan extension, as reported in a recent study that linked decreased neuronal excitability to longevity in humans and *C. elegans* [25].

DAF-2 muscle signaling impairs mobility from mid-adulthood

Muscle inactivation of DAF-2 did not affect the BBF of 1-day-old adult animals **(Figure 5a)**, but was sufficient to recapitulate the higher BBF of 13-day-old adult animals with ubiquitous DAF-2 depletion **(Figure 5c)**. Furthermore, inactivation of DAF-2 in both muscles and neurons did not significantly affect the impact of DAF-2 depletion in muscles in 13-day-old adults (Figure 5c). Thus, the increase in motility associated with DAF-2 inactivation in muscles did not depend on the status of DAF-2 in other tissues, including neurons. These data corroborate the results obtained with the DAF-16::wrmSCARLET reporter **(Figure 4d, e)** and show that DAF-2 functions autonomously in the muscle to control worm mobility in middle age. Finally, DAF-2 muscle activity can also be uncoupled from the regulation of lifespan and resistance of worms to oxidative stress **(Figure 2a,b and Figure S2d).**

Both neuronal and muscular DAF-2 depletion prevents muscle mitochondria fragmentation with age.

We and others have previously shown that the morphology of muscle mitochondria changes from an interconnected to a fragmented network during muscle ageing and that this phenotype is associated with loss of mobility in old age[24]. To further investigate the cell autonomous function of DAF-2 in muscle ageing, we monitored the muscle mitochondria pattern with age. We visualized mitochondria by expressing a single-copy insertion of a reporter encoding the N-terminal segment of TOM20 (responsible for its anchoring to the mitochondrial outer membrane) fused to the fluorescent protein wrmSCARLET, under the control of the muscle *pmyo-3* promoter (see Experimental procedures). It is noticeable that previously characterized worm strains carrying similar reporters but as an integrated multicopy array showed earlier mitochondrial fragmentation, probably due to overexpression of the fusion protein [24,26]. The ubiquitous degradation of DAF-2 delayed the fragmentation of mitochondria

(Figure 6) in agreement with previous observations with the *daf-2(e1370)* mutant [24]. Muscle inactivation of DAF-2 was sufficient to prevent muscle mitochondria fragmentation. However, neuronal depletion of DAF-2 gave similar results, alone or in combination with muscle depletion of DAF-2 **(Figure 6).** Thus, inactivation of DAF-2 in muscles or neurons is sufficient to prevent mitochondrial fragmentation, suggesting that DAF-2 acts both autonomously and non-autonomously to maintain muscle integrity during ageing.

CONCLUSION

Overall, we have developed a powerful tool to explore DAF-2 function with ageing, uncovering unexpected findings regarding tissue-specific roles of DAF-2 in the regulation of dauer, lifespan, resistance to oxidative stress, and mobility, as well as in the cross-talk between tissues. Our data revealed that the mobility phenotype of *daf-2* mutants results from the balance between different tissue-specific DAF-2 activities whose contribution varies with ageing. Many phenotypes have been associated with *daf-2* mutants and the future challenge will be to determine the role of the different tissue-specific activities of DAF-2 in the regulation of these phenotypes and their downstream effectors.

Figure legends

Figure 1: Expression pattern of DAF-2::AID::mNG and functional validation of its degradation by the auxin-inducible system

(a) Image of DAF-2::AID::mNG in 1-day-old *daf-2(kr462)* adult. Scale bar: 100 µm. **(b)** Survival curves of control (N2) and *daf-2(kr462)* animals (N= 2, n= 141 and 138 for N2 and *daf-2(kr462)*, respectively). **(c)** Survival curves of N2, *daf-2(e1370)* mutants, and worms with ubiquitous depletion of DAF-2. Data have been pooled from two independent experiments (n=155-160 for each genotype, see Table S2 for detailed lifespan data and statistics) in which two different *Peft-3::*TIR1 containing strains were tested (see Table S1 for strain description). **(d-e)** Body bends frequency at day 1 **(d)** and day 13 **(e)** of adulthood of N2, *daf-2(e1370)* or *daf-2(kr462)* worms, with or without ubiquitous expression of TIR1. The number of animals scored is indicated in each bar and corresponds to the pool of two experiments (see Figure 5 for more replicates). Bars indicate median values, means are represented by black horizontal lines and brackets show standard deviations, ns: non-significant, ***: $p < 0.001$, Kruskal-Wallis and Dunn's post hoc test with FDR method for adjusting p-value. All experiments were performed at 20°C.

Figure 2: DAF-2::AID::mNG is effectively downregulated in the presence of ubiquitously expressed TIR1 after auxin treatment

(a-g) Images of DAF-2::AID::mNG in 1-day-old *daf-2(kr462)* adults expressing ubiquitous TIR1 and grown in the absence of auxin (upper panels) or after 24 hours of auxin treatment (lower panels). Images focus on specific body regions: the head **(a)**, showing strong expression in the nerve ring (NR) and the XXX cells; the neuronal cell bodies of the ventral nerve cord (VNC) **(b)**; the proliferating germ cells **(c)**, the embryos **(d)**, the epidermal syncytium **(e)**, the intestine **(f)** and the body wall muscles **(g)**. For the intestine **(f)**, images are taken in *apb-3(ok429)* mutant background in order to reduce unspecific intestinal autofluorescence (arrows indicate the specific DAF-2::AID::mNG associated signal). In all images, the remaining staining of the gut after auxin treatment corresponds to non-specific autofluorescence that varies between animals. Similar results were obtained in 7-day-old animals (data not shown). Scale bars: 20 µm.

Figure 3: Inactivation of DAF-2 in neurons or in the gut is sufficient to increase lifespan

(a-k) Survival curves of animals with DAF-2 depletion in all cells **(a-k)**, muscles **(a-b)**, germline **(c-d)**, epidermis **(e-f)**, intestine **(g-h)**, neurons **(i-j)** or neurons and intestine **(k)**. Numbers (ex: Muscle 1, Muscle 2) refer to distinct alleles driving TIR1 expression (See Sup Table 1 for complete strain description). Some experiments were split in separate graphs for clarity, thus some graphs share the

same negative and positive controls: **(a)**, **(e)** and **(i)**; **(b)** and **(d)**; **(c)** and **(g)**; **(f)** and **(h)**. The control conditions correspond to the N2 or *daf-2(kr462)* strains, in the presence of EtOH or auxin, whose lifespans did not show significant differences. For detailed data on lifespan, replicates and statistics, see Supplementary Table 2. **(l-n)** Survival curves of animals with DAF-2 depletion in all cells (**l-n**, n=265), intestine (**l,** n=75 for each line), neurons (**m**, n=100 for each line) or neurons and intestine (**n**, n=90 for each line) in presence of 20 mM paraquat. Controls correspond to *daf-2(kr462)*. All strains including controls have been treated with auxin. Three independent experiments were performed in which two independent lines for intestinal, neuronal or ubiquitous DAF-2 depletion were used. For detailed replicates and statistics, see Supplementary Table 2.

Figure 4: **Regulation of DAF-16 subcellular localisation by tissue-specific depletion of DAF-2**

(a-e) Images of DAF-16::wSCARLET in the head (left and middle panels) or the anterior body (right panels) of 1-day-old *daf-16(kr535); daf-2(kr462)* adults without (a) or with ubiquitous (b), intestinal (c), neuronal (d) or muscular (e) depletion of DAF-2 caused by 24 hours of auxin treatment (b-e). Empty arrowheads, full arrows and empty arrows indicate muscle, neuron and intestinal nuclei respectively; full arrowheads correspond to the cytosol of neurons. For numbers and percentage of worms with a strong DAF-16::wSCARLET nuclear signal, see supplementary Table 4.

Figure 5: DAF-2 degradation in neurons or muscles differentially alters mobility in an age-dependent manner

(a-c) Body bends frequency of 1-day-old **(a-b)** and 13-day-old **(c)** adults with depletion of DAF-2 in all cells or in the intestine, muscle, neurons or muscle and neurons as indicated. Control corresponds to *daf-2(kr462)* in presence of auxin. Numbers (ex: Muscle 1, Muscle 2) refer to distinct alleles driving TIR1 expression (See Sup Table 1 for the description of strains). **(a and c)** Pooled data from five independent experiments. Control strains from all replicates were included and each independent tissue-specific strain was tested at least once. **(b)** Pooled data from three independent experiments. The number of animals scored is indicated in each bar. The bars correspond to the median values, the means are represented by black horizontal lines and brackets show standard deviations. Comparisons were done with Kruskal-Wallis, Dunn post-hoc tests with FDR method to adjust p-value, ns: not significant, ***: $p_{adjusted} < 0.001$. Statistics are presented as two lines that include comparison with the control strain or with one specific strain (ubiquitous 1 or neuron 2 for **(a and c)** and **(b)** respectively).

Figure 6: Muscle or neuronal depletion of DAF-2 is sufficient to prevent mitochondria fragmentation

(a-c) Quantification of muscular mitochondrial morphology at day 14 **(a)**, day 17 **(b)**, or day 21 **(c)** of adulthood in worms with DAF-2 depletion in all tissues, or in muscle, neurons or muscle and neurons as indicated. The number of animals scored is indicated in each bar. Data correspond to a pool of three to five independent trials depending on the strain. Strains used were: *daf-2(kr462)* in presence of auxin as Control, Ubiquitous 1, Neuron 1 and 2, Muscle 1, Muscle 1 + Neuron 1 (see Sup Table 1 for strain description). Comparisons used Fisher exact test, followed by pairwise tests with FDR adjusting method as post-hoc tests: ns: not significant, *: $p_{adjusted} < 0.05$, ***: $p_{adjusted} < 0.001$. Statistics are presented as two lines that include comparison with the control and Ubiquitous 1 strain.

Supplementary Figure 1 associated with figure 2: DAF-2::AID::mNG is efficiently degraded in different tissues in presence of auxin upon TIR1 expression driven by tissue specific promoter.

(a-g) Images of DAF-2::AID::mNG expression in adult animals at day 1. Animals express transgenic TIR1 under the control of tissue specific promoters, as indicated, in the absence (upper panel) or in the presence (lower panel) of 1 mM auxin for 24 hours. **(a-b)** With a neuronal promoter, DAF-2::AID::mNG was no longer detected in the nerve ring (NR) **(a)** and in the ventral nerve cord (VNC) **(b)** but was still detected in the XXX cell **(a)**. **(c-d)** With a germline promoter, DAF-2::AID::mNG signal was reduced in the proliferating germ cells **(c)** and in the eggs **(d)**. **(e)** With a epidermal promoter, DAF-2::AID::mNG disappeared from the epidermis syncytium. **(f)** With a muscular promoter, DAF-2::AID::mNG disappeared from body wall muscles. **(g)** With an intestinal promoter, DAF-2::AID::mNG signal was downregulated in the intestine. *apb-3(ok429)* mutants with reduced intestinal autofluorescence were used. Scale bars: 20 µm **(a-f)**, 10 µm **(g)**.

Supplementary Figure 2 associated to figure 3: Muscle DAF-2 depletion did not confer resistance to oxidative stress

Survival curves of animals with DAF-2 depletion in all cells or in muscles in presence of 20 mM paraquat. Controls correspond to *daf-2(kr462)*. All strains including controls have been treated with auxin from the L4 stage. Two independent experiments were performed in which two independent lines for muscle or ubiquitous DAF-2 depletion were used. For detailed replicates and statistics, see Supplementary Table 2.

Table S1: Strains description

Table S2: Replicates and statistics for lifespan measurements

Table S3: Regulation of dauer arrest in worms with tissue-specific depletion of DAF-2

Table S4: Numbers and proportion of worms with DAF-16::wrmSCARLET nuclear accumulation

Table S5: Plasmids and alleles generated

Experimental Procedures

C. elegans strains and media

All experiments were performed at 20°C except where specified. All strains were maintained at 20°C, except strain FS428 *daf-2(e1370)* III (corresponding to the original CB1370 strain crossed 6 times) which was maintained at 19°C to prevent larval arrest. Strains were grown on nematode growth medium (NGM) agar plates freshly poured and seeded with *Escherichia coli* OP50 culture. The wild-type reference strain was *C. elegans* N2 Bristol. All strains used in this study are described in Table S1.

Plasmids and generation of single-copy insertion alleles

The plasmids constructed for this study are described in Table S5. Plasmids used to create single copy insertion alleles by the miniMos method[27] are described in previous studies [28,29] and the newly generated alleles are listed in Table S5. All constructs were verified by Sanger sequencing from GATC Company. For tissue specific expression, the promoters used were: myo-3– (body-wall muscle), unc-47– (GABAergic motoneuron), unc-17– (cholinergic motoneuron), rab-3– (pan-neuronal), dpy-7– (epidermis), or eft-3– (ubiquitous), N2 animals were injected with 15 ng/µl plasmid of interest containing the promoter and the open reading frame TIR1 or TOMM20 fused to fluorescent proteins, 50 ng/µl pCFJ601 (Mos1 transposase), 10 ng/µl pMA122 (negative selective marker Phsp16.2::peel-1), and 2.5 ng/µl pCFJ90 (Pmyo-2::mCherry). Neomycin (G418) was added to plates 24 h after injection at 1.5 µg/µl final concentration. Candidate plates were heat shocked for 2 h at 34°C. Selected lines were then bred to homozygosity and then crossed to generate the desired strains.

Alleles generation by CRISPR/cas9 genome engineering

To generate the *kr462* allele, a flexible linker, the AID sequence[17], another flexible linker and mNeonGreen were inserted tandemly into the *daf-2* locus, just before the stop codon. This sequence was PCR amplified with or without homology arms from pCR12 and the PCR products were used to generate the repair template [30]. To generate the *kr535* allele, a flexible linker, the wrmScarlet [31], another flexible linker and 3 MYC tags were inserted tandemly into the *daf-16* locus, just before the stop codon. This sequence was PCR amplified with or without homology arms and the PCR products were used to generate the repair template[30]. CrRNA were designed on *Benchling.com* and synthesized by IDT (Integrated DNA Technologies). For *kr462* TGAAAATGAGCATCTAATCG and ttttgggggttTCAGACAAG crRNA were used in tandem, for *kr535* CATGAGCTGAGTCAAGCTGG and tctctttcgaacaacaccag were used in tandem. The injection mix contained annealed double-stranded

DNA donor cocktail as repair template at 200 ng/µl, Cas9 nuclease at 0.25 µg/µl (Integrated DNA Technologies), tracrRNA-crRNA duplex at 9 µM, pRF4 [*Peft- 3::rol-6*] coinjection marker at 2.5 ng/µl, and RNase/DNase-free water qsp 20 µl. The candidate F1 animals were isolated by tracking the initial fluorescence knock-in in plates with F1 roller progeny. The F2 progenies were then isolated and homozygosed. The insertion was then confirmed by PCR and sequencing. Candidates were then outcrossed once with N2 before further crosses to generate the desired strains (See Table S1).

Ageing cohorts and auxin treatment

Auxin plates were prepared by adding auxin indole-3-acetic acid (Sigma-Aldrich) from a 400 mM stock solution in ethanol into NGM at the final concentration of 1 mM[17]. For control ethanol plates, the same volume of ethanol was added to NGM. Animals were transferred on auxin or ethanol plates at the L4 stage except for dauer tests for which eggs were laid and grown on auxin or ethanol plates.

For all ageing cohorts, 20 µM 5-fluorouracil (5-FU, Sigma-Aldrich) was added to prevent progeny growth. Animals were transferred weekly to fresh plates, without 5-FU after two weeks. The day of transition to L4 is counted as day 0 of adulthood for the cohort.

Dauer and Lifespan assays

For dauer assays, L4s were transferred to ethanol or 1 mM auxin plates and allowed to mature into egg-laying adults, then removed after twenty-four hours. Progeny were assessed after forty-eight hours at 25°C for the presence of dauer larvae.

For lifespan assays, cohorts were handled as described in “ageing cohorts”. Lifespans were conducted at 20°C and were assessed every 2–3 days as described previously[32]. Briefly, animals were scored as dead when they stopped moving and responding to prodding, they were censored when they crawled off the plate, had a “protruding vulva” or an “exploded vulva”. For oxidative stress survival assays, animals were transferred to 1 mM auxin plates at the L4 stage. After seven hours, young adult animals were transferred to 1 mM auxin plates supplemented with 20 mM paraquat (Methyl viologen dichloride hydrate, Sigma-Aldrich). Animals were scored as in lifespan assays but twice a day. All lifespan tests were blinded to avoid bias in the evaluation.

Thrashing assays

For body bends frequency (BBF) measurements, 1-day-old or 13-day-old worms prepared as described in “ageing cohorts” were gently transferred into a 12-wells cell culture plate (ten worms per well) containing 1.5 mL of 2 % agarose in M9 buffer (3 g KH2PO4, 6 g Na2HPO4, 5 g NaCl, 0.25 g MgSO4·7 H2O, and distilled water up to 1 liter) and 2 mL of M9 buffer per well. One minute after transfer, animal

movements were recorded for 30 s. BBF was then quantified using the open-source wrMTrck plugin on Fiji (ImageJ (v2.0.0)) software.

Microscopy and image processing

For all observations, animals were mounted on 2 % agarose dry pads with 4 % polystyrene beads (Polybeads, Polysciences) in M9 buffer. For images corresponding to Figure 1a, 2 and 4, worms were observed using an Andor spinning disk system (Oxford Instruments) installed on a Nikon-IX86 microscope (Olympus) equipped with a 40x/NA 1.3 and a 60×/NA 1.42 oil-immersion objectives and an Evolve electron-multiplying charge-coupled device camera. Each animal was imaged with IQ software (APIS Informationstechnologien) as a stack of optical sections (0.3 µm apart) across the whole thickness of the worm (Figure 1A) or across a specific tissue (Figure 2 and 4). All images were processed using the Fiji (ImageJ) software and correspond to the sums of the same number of slices (for each strain with or without auxin) except for images of the intestine (Figure 2(g) and S1(h)) and Figure 4 which correspond to z projection of maximum intensity.

Scoring of DAF-16 nuclear localization

One-day-old adults were observed using a AZ100 Multizoom Microscope (Nikon) equipped with a CMOS flash 4 C11440 (Hamammatsu) camera, for no more than 10 minutes per slide to avoid post-mounting DAF-16::wSCARLET nuclear translocation. In absence of auxin, the fluorescence associated with DAF-16::wSCARLET appeared diffuse in the cytoplasm and nuclei of most tissues, except in the head neurons where it was completely excluded from the nuclei. A tissue was scored positive when several nuclei were brighter than the cytoplasm. Strains scoring and image analysis were performed blind.

Scoring of muscle mitochondria morphology

Images of *krSi134*[Pmyo-3::tom-20N::wScarlet] worms were acquired on an Axioscop compound microscope (Zeiss) equipped with a Neofluar 63x/NA 1.25 oil-immersion objective and a EMCC CoolSnap HQ (Photomectrics) camera. For each worm a representative image from the posterior body wall muscle cells was acquired. Cells with long interconnected mitochondrial networks were classified as interconnected; cells with a combination of interconnected mitochondrial networks along with some smaller fragmented mitochondria were classified as interrupted; cells with sparse small round mitochondria were classified as fragmented. Strains scoring and image analysis were performed blind.

Statistical analysis

All statistical analyses were performed with R version 4.0.1 (2020-06-06). The R Test Survival Curve Differences (package survival_3.2-3) was used to analyze lifespan assays. This test is based on the *G-rho* family of tests which makes use of the Kaplan-Meier estimate of survival[33]. Thrashing assays were analyzed using the non-parametric Kruskal-Wallis Rank Sum Test, followed by Dunn's Test of Multiple Comparisons (package rstatix_0.6.0) with FDR adjusting method as post-hoc tests. To compare between different conditions for the mitochondria morphology assay a Fisher exact test was performed, followed by pairwise tests with FDR adjusting method as post-hoc tests (package rcompanion_2.4.1). For all tests compared samples were considered different when statistical test gave an adjusted P-value <0.05 (*p<0.05; **p<0.01; ***p<0.001), ns: non-significant.

References

1. Kenyon, C., Chang, J., Gensch, E., Rudner, A. & Tabtiang, R. A C. elegans mutant that lives twice as long as wild type. *Nature* **366**, 461–464 (1993).
2. Kenyon, C. J. The genetics of ageing. *Nature* **464**, 504–512 (2010).
3. Lin, K., Dorman, J. B., Rodan, A. & Kenyon, C. daf-16: An HNF-3/forkhead family member that can function to double the life-span of Caenorhabditis elegans. *Science* **278**, 1319–1322 (1997).
4. Ogg, S. *et al.* The Fork head transcription factor DAF-16 transduces insulin-like metabolic and longevity signals in C. elegans. *Nature* **389**, 994–999 (1997).
5. Henderson, S. T. & Johnson, T. E. daf-16 integrates developmental and environmental inputs to mediate aging in the nematode Caenorhabditis elegans. *Curr. Biol. CB* **11**, 1975–1980 (2001).
6. Lee, R. Y., Hench, J. & Ruvkun, G. Regulation of C. elegans DAF-16 and its human ortholog FKHRL1 by the daf-2 insulin-like signaling pathway. *Curr. Biol. CB* **11**, 1950–1957 (2001).
7. Lin, K., Hsin, H., Libina, N. & Kenyon, C. Regulation of the Caenorhabditis elegans longevity protein DAF-16 by insulin/IGF-1 and germline signaling. *Nat. Genet.* **28**, 139–145 (2001).
8. Li, W.-J. *et al.* Insulin signaling regulates longevity through protein phosphorylation in Caenorhabditis elegans. *Nat. Commun.* **12**, 4568 (2021).
9. Tepper, R. G. *et al.* PQM-1 complements DAF-16 as a key transcriptional regulator of DAF-2-mediated development and longevity. *Cell* **154**, 676–690 (2013).
10. Hahm, J.-H. *et al.* C. elegans maximum velocity correlates with healthspan and is maintained in worms with an insulin receptor mutation. *Nat. Commun.* **6**, 8919 (2015).
11. Liu, J. *et al.* Functional Aging in the Nervous System Contributes to Age-Dependent Motor Activity Decline in C. elegans. *Cell Metab.* **18**, 392–402 (2013).
12. Mulcahy, B., Holden-Dye, L. & O'Connor, V. Pharmacological assays reveal age-related changes in synaptic transmission at the *Caenorhabditis elegans* neuromuscular junction that are modified by reduced insulin signalling. *J. Exp. Biol.* jeb.068734 (2012) doi:10.1242/jeb.068734.
13. Kimura, K. D., Riddle, D. L. & Ruvkun, G. The C. elegans DAF-2 Insulin-Like Receptor is Abundantly Expressed in the Nervous System and Regulated by Nutritional Status. *Cold Spring Harb. Symp. Quant. Biol.* **76**, 113–120 (2011).
14. Wolkow, C. A., Kimura, K. D., Lee, M.-S. & Ruvkun, G. Regulation of C. elegans Life-Span by Insulinlike Signaling in the Nervous System. **290**, 5 (2000).
15. Libina, N., Berman, J. R. & Kenyon, C. Tissue-Specific Activities of C. elegans DAF-16 in the Regulation of Lifespan. *Cell* **115**, 489–502 (2003).
16. Uno, M. *et al.* Neuronal DAF-16-to-intestinal DAF-16 communication underlies organismal lifespan extension in C. elegans. *iScience* **24**, 102706 (2021).
17. Zhang, L., Ward, J. D., Cheng, Z. & Dernburg, A. F. The auxin-inducible degradation (AID) system enables versatile conditional protein depletion in C. elegans. *Dev. Camb. Engl.* **142**, 4374–4384 (2015).
18. Gems, D. *et al.* Two Pleiotropic Classes of daf-2 Mutation Affect Larval Arrest, Adult Behavior, Reproduction and Longevity in Caenorhabditis elegans. *Genetics* **150**, 129–155 (1998).
19. Dillin, A., Crawford, D. K. & Kenyon, C. Timing Requirements for Insulin/IGF-1 Signaling in. **298**, 6 (2002).
20. Venz, R., Pekec, T., Katic, I., Ciosk, R. & Ewald, C. Y. End-of-life targeted degradation of DAF-2 insulin/IGF-1 receptor promotes longevity free from growth-related pathologies. *eLife* **10**, e71335 (2021).
21. Aghayeva, U. *et al.* DAF-16/FoxO and DAF-12/VDR control cellular plasticity both cell-autonomously and via interorgan signaling. *PLOS Biol.* **19**, e3001204 (2021).
22. Honda, Y. & Honda, S. Oxidative stress and life span determination in the nematode Caenorhabditis elegans. *Ann. N. Y. Acad. Sci.* **959**, 466–474 (2002).
23. Duhon, S. A. & Johnson, T. E. Movement as an index of vitality: comparing wild type and the age-1 mutant of Caenorhabditis elegans. *J. Gerontol. A. Biol. Sci. Med. Sci.* **50**, B254-261 (1995).

24. Mergoud dit Lamarche, A. *et al.* UNC-120/SRF independently controls muscle aging and lifespan in *Caenorhabditis elegans*. *Aging Cell* **17**, e12713 (2018).
25. Zullo, J. M. *et al.* Regulation of lifespan by neural excitation and REST. *Nature* **574**, 359–364 (2019).
26. Regmi, S. G., Rolland, S. G. & Conradt, B. Age-dependent changes in mitochondrial morphology and volume are not predictors of lifespan. *Aging* **6**, 118–130 (2014).
27. Frøkjær-Jensen, C. *et al.* Random and targeted transgene insertion in Caenorhabditis elegans using a modified Mos1 transposon. *Nat. Methods* **11**, 529–534 (2014).
28. Zhou, X. *et al.* The netrin receptor UNC-40/DCC assembles a postsynaptic scaffold and sets the synaptic content of GABAA receptors. *Nat. Commun.* **11**, 2674 (2020).
29. Zhou, X. *et al.* The HSPG syndecan is a core organizer of cholinergic synapses. *J. Cell Biol.* **220**, e202011144 (2021).
30. Dokshin, G. A., Ghanta, K. S., Piscopo, K. M. & Mello, C. C. Robust Genome Editing with Short Single-Stranded and Long, Partially Single-Stranded DNA Donors in *Caenorhabditis elegans*. *Genetics* **210**, 781–787 (2018).
31. El Mouridi, S. *et al.* Reliable CRISPR/Cas9 Genome Engineering in Caenorhabditis elegans Using a Single Efficient sgRNA and an Easily Recognizable Phenotype. *G3 Bethesda Md* **7**, 1429–1437 (2017).
32. Masse, I. *et al.* A Novel Role for the SMG-1 Kinase in Lifespan and Oxidative Stress Resistance in Caenorhabditis elegans. *PLoS ONE* **3**, e3354 (2008).
33. Fleming, T. R., Green, S. J. & Harrington, D. P. Performing serial testing of treatment effects. *Experientia. Suppl.* **41**, 469–484 (1982).

(a) **DAF-2::AID::mNG**

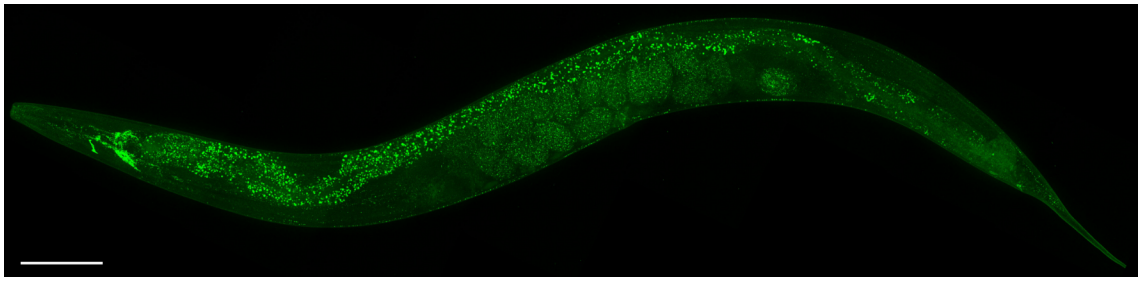

(b)

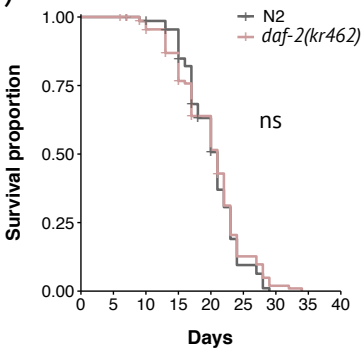

(c)

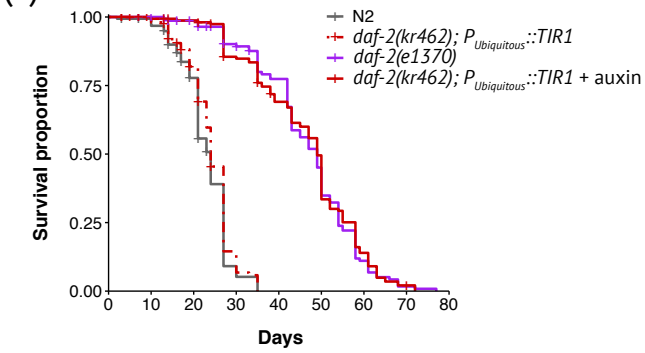

(d)

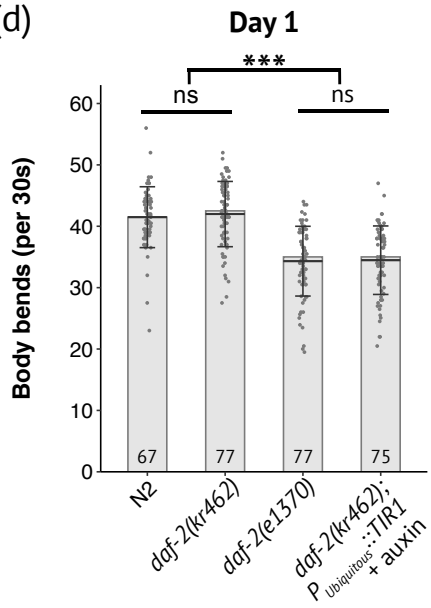

(e)

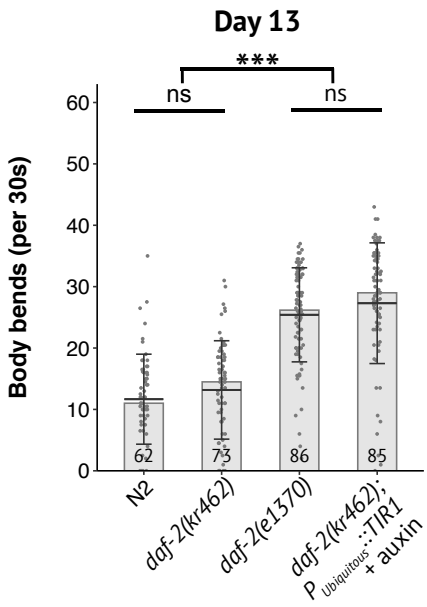

Figure 1

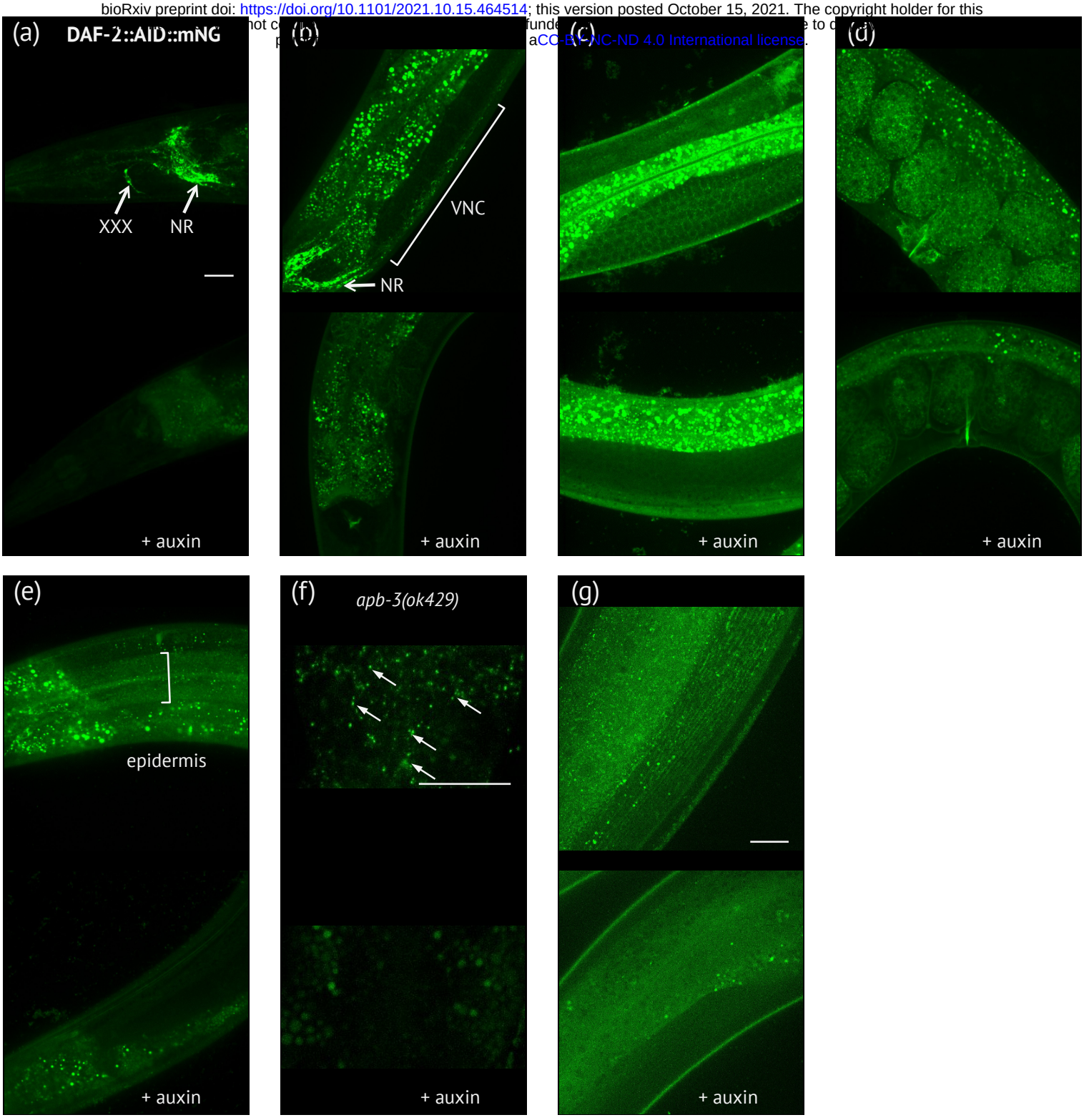

Figure 2

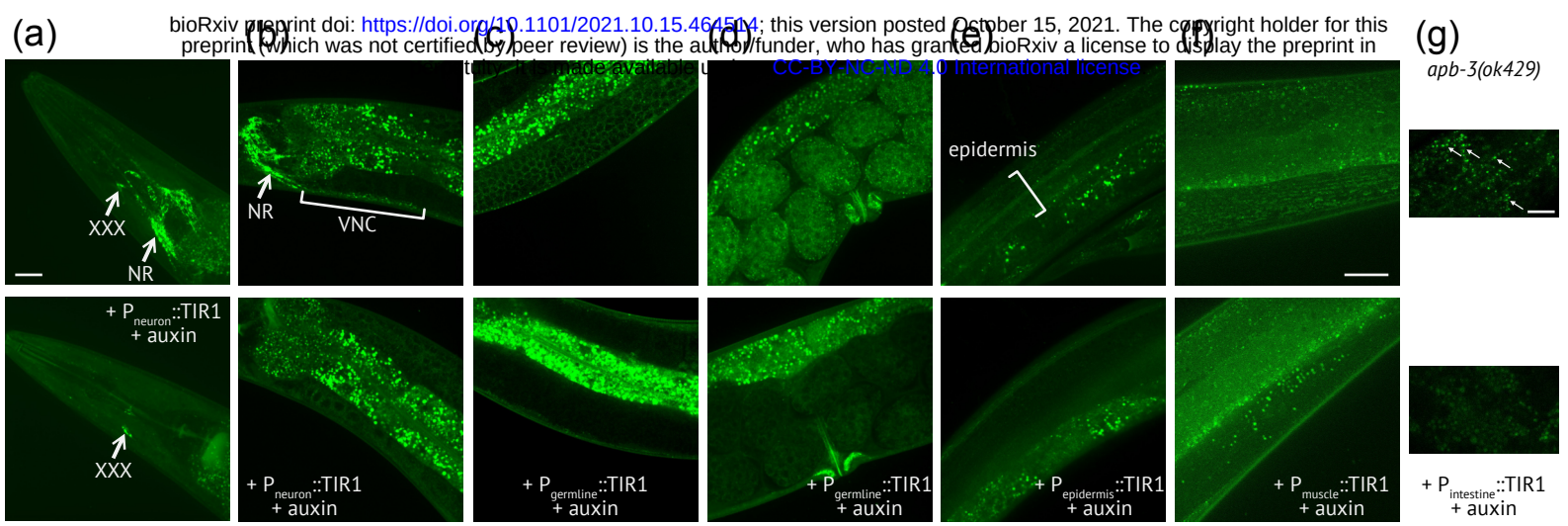

Supplementary Figure 1 associated to figure 2

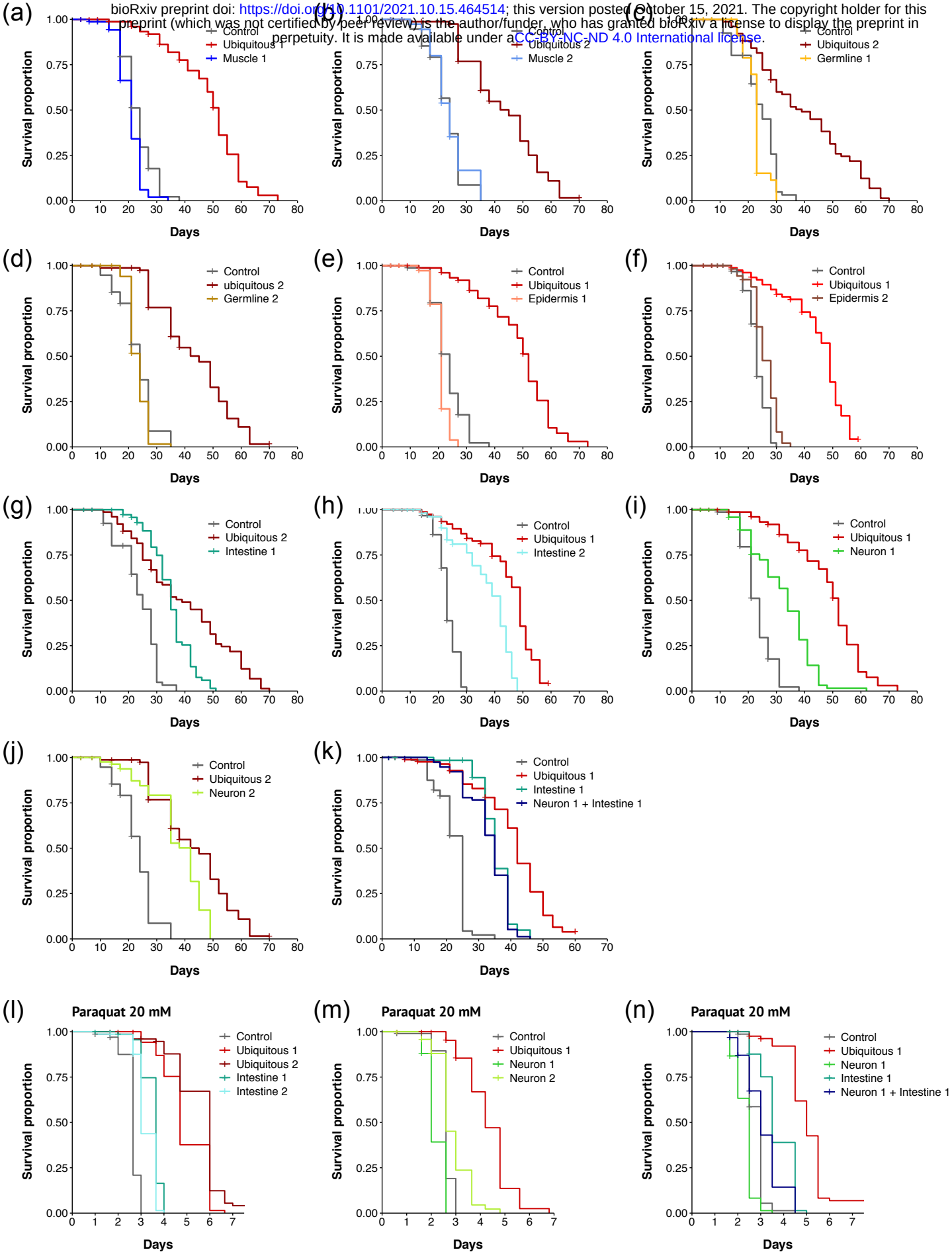

Figure 3

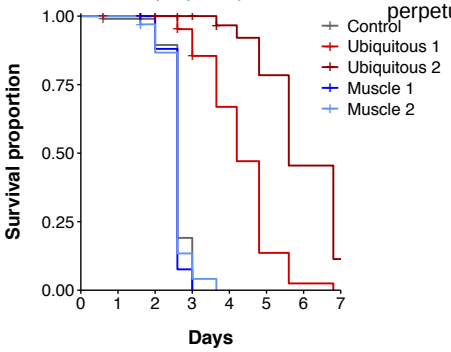

Supplementary Figure 2 associated to figure 3

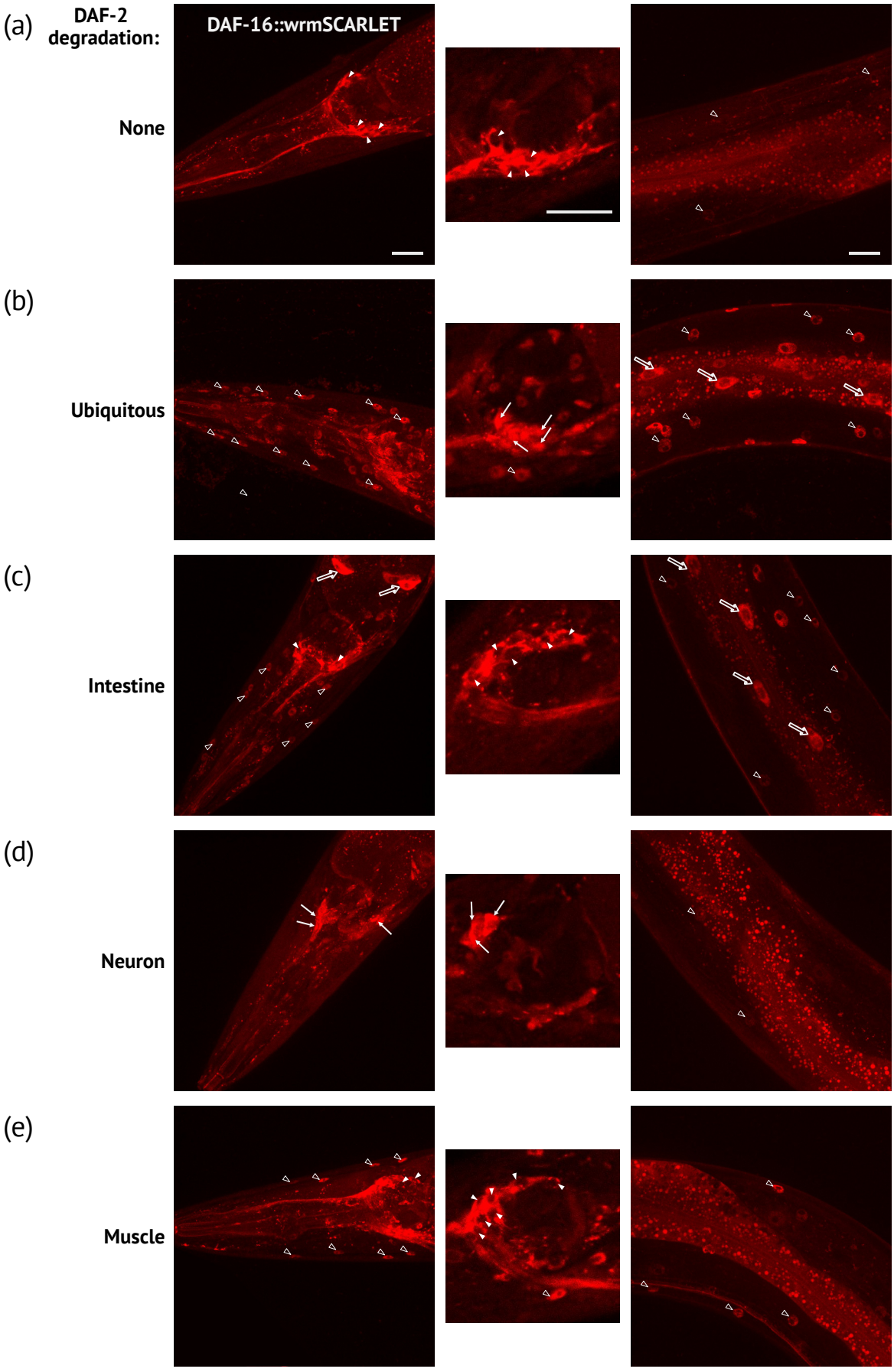

Figure 4

(a)

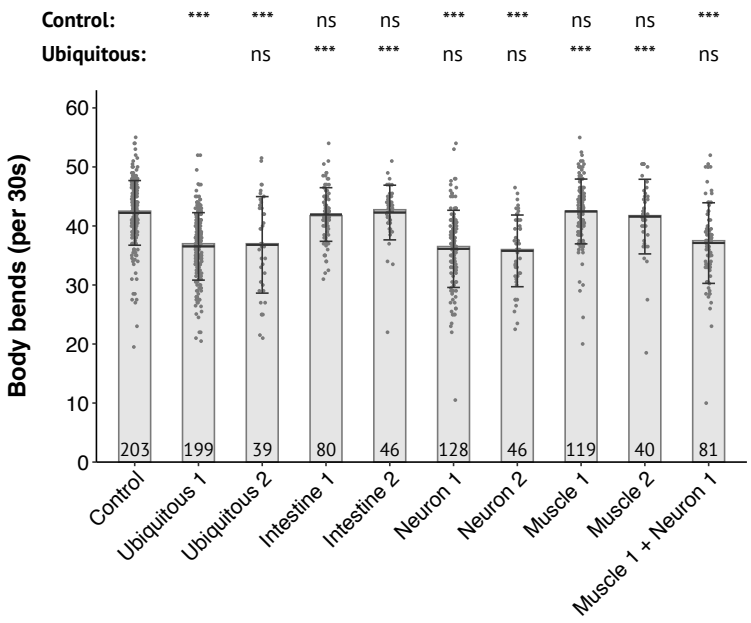

(b)

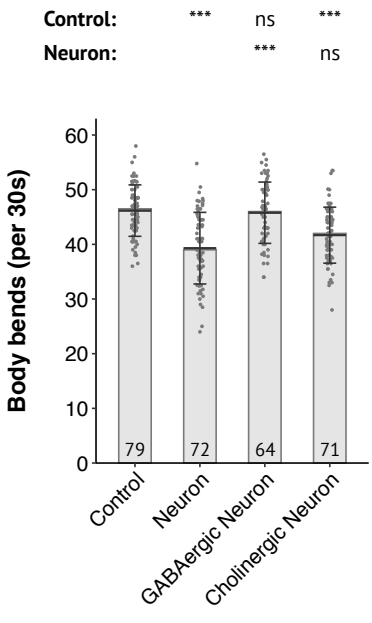

(c)

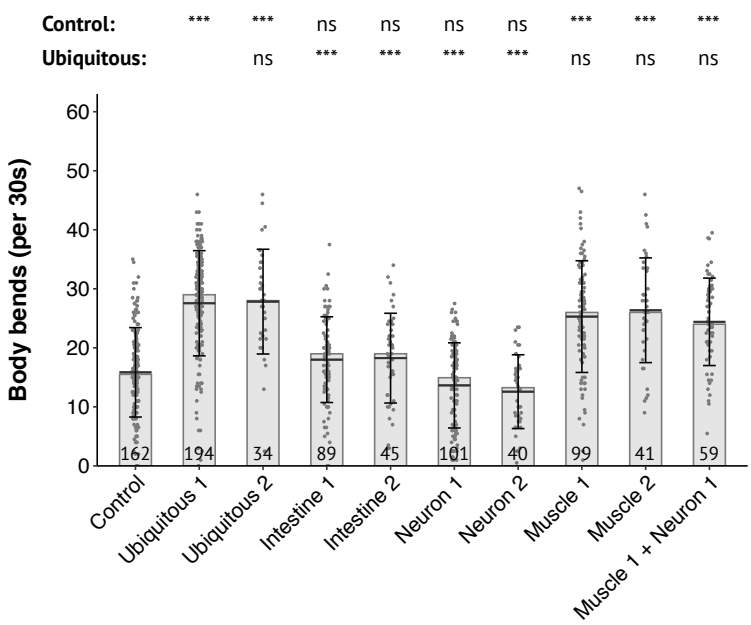

Figure 5

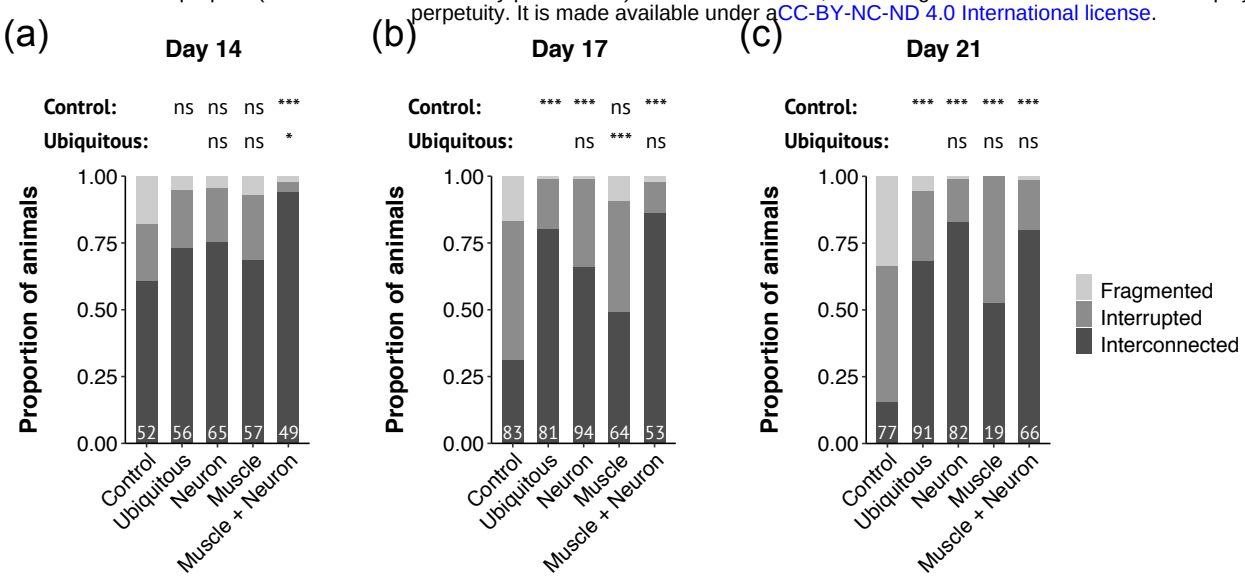

Figure 6

Table S1: Strains

Strains	Genotypes	Promotor driving TIR1 expression	Tissues with DAF-2 degradation	Source of TIR1 alleles
EN7563	*kr462[daf-2::linker::AID::linker::mNeonGreen] III; krSi50[Peft-3::TIR1::tagBFP] IV*	*eft-3*	Ubiquitous 1	Zhou et al., 2021
EN7863	*kr462 III; krSi45[Peft-3::TIR1::tagBFP] V*	*eft-3*	Ubiquitous 2	This work
EN7565	*kr462 III; krSi55[Pmyo-3::TIR1::tagBFP] V*	*myo-3*	Muscle 1	Zhou et al., 2021
EN7864	*krSi81[Pmyo-3::TIR1::tagBFP] I; kr462 III*	*myo-3*	Muscle 2	This work
EN7567	*kr462 III; krSi36[Prab-3::TIR1::tagBFP] V*	*rab-3*	Neuron 1	Zhou et al., 2021
EN7865	*kr462 III; krSi140[Prab-3::TIR1::tagBFP] IV*	*rab-3*	Neuron 2	This work
EN7691	*ieSi61[Pges-1::TIR1::mRuby + Cbr-unc-119(+)] II; kr462 III*	*ges-1*	Intestine 1	Zhang et al., 2015
EN8173	*reSi5[Pges-1::TIR1::F2A::mTagBFP2::NLS::AID::tbb-2 3'UTR] I; kr462 III*	*ges-1*	Intestine 2	Guinevere Ashley et al. Biorxiv 2020
EN7569	*krSi63[Pdpy-7::TIR1::tagBFP] II; kr462 III*	*dpy-7*	Epidermis 1	Zhou et al., 2021
EN8032	*kr462 III, krSi53[Pdpy-7::TIR1::tagBFP] III*	*dpy-7*	Epidermis 2	This work
EN7861	*kr462 III; ieSi38[Psun-1::TIR1::mRuby::sun-1 3'UTR + Cbr-unc-119(+)] IV*	*sun-1*	Germline 1	Zhang et al., 2015
EN7862	*ieSi68[Psun-1::TIR1::mRuby::htp-1 3'UTR + Cbr-unc-119(+)] II; kr462 III*	*sun-1*	Germline 2	Zhang et al., 2015
EN7964	*ieSi61[Pges-1::TIR1::mRuby + Cbr-unc-119(+)] II; kr462 III; krSi36[Prab-3::TIR1::tagBFP] V*	*ges-1 + rab-3*	Intestine 1 + Neuron 1	Zhang et al., 2015; Zhou et al., 2021
EN7737	*kr462 III; krSi36[Prab-3::TIR1::tagBFP] V, krSi55[Pmyo-3::TIR1::tagBFP] V*	*rab-3 + myo-3*	Neuron 1 + Muscle 1	Zhou et al., 2021
EN8491	*kr462 III; krSi51[Punc-47::TIR1::BFP] IV*	*unc-47*	GABAergic neuron	This work
EN8492	*kr462 III; krSi52[Punc-17::TIR1::BFP]*	*unc-17*	Cholinergic neuron	This work
EN8113	*kr535[daf-16::linker::wScarlet::linker::3xMYC] I; kr462 III; krSi50[Peft-3::TIR1::tagBFP] IV*	*eft-3*	Ubiquitous 1	Zhou et al., 2021
EN8169	*kr535[daf-16::linker::wScarlet::linker::3xMYC] I; kr462 III; krSi140[Prab-3::TIR1::tagBFP] IV*	*rab-3*	Neuron 2	This work
EN8170	*kr535[daf-16::linker::wScarlet::linker::3xMYC] I; kr462 III; krSi55[Pmyo-3::TIR1::tagBFP] V*	*myo-3*	Muscle 1	Zhou et al., 2021
EN8536	*kr535[daf-16::linker::wScarlet::linker::3xMYC] I; ieSi61[Pges-1::TIR1::mRuby + Cbr-unc-119(+)] II; kr462 III*	*ges-1*	Intestine 1	Zhang et al., 2015
EN7878	*krSi134[Pmyo-3::tom-20N::wScarlet] I; kr462 III; krSi50[Peft-3::TIR1::tagBFP] IV*	*eft-3*	Ubiquitous 1	Zhou et al., 2021
EN8315	*krSi134[Pmyo-3::tom-20N::wScarlet] I; kr462 III; krSi55[Pmyo-3::TIR1::tagBFP] V*	*myo-3*	Muscle 1	Zhou et al., 2021
EN8316	*krSi134[Pmyo-3::tom-20N::wScarlet] I; kr462 III; krSi140[Prab-3::TIR1::tagBFP] IV*	*rab-3*	Neuron 2	This work
EN8489	*krSi134[Pmyo-3::tom-20N::wScarlet] I; kr462 III; krSi36[Prab-3::TIR1::tagBFP] V*	*rab-3*	Neuron 1	Zhou et al., 2021
EN8490	*krSi134[Pmyo-3::tom-20N::wScarlet] I; kr462 III; krSi36[Prab-3::TIR1::tagBFP] V, krSi55[Pmyo-3::TIR1::tagBFP] V*	*rab-3 + myo-3*	Neuron 1 + Muscle 1	Zhou et al., 2021

Other strains used in this study

Strains	Genotypes	Source
N2	*wt*	CGC
FS428	*daf-2(e1370) III (CB1370 outcrossed 6x)*	Mergoud et al., 2018
EN462	*kr462[daf-2::linker::AID::linker::mNeonGreen] III*	This work
EN50535	*kr535[daf-16::linker::wScarlet::linker::3xMYC] I*	This work
EN8313	*krSi134[Pmyo-3::tom-20N::wScarlet] I; kr462 III*	This work

Table S2: Lifespan measurements

Experiment number	Corresponding Figure	Strain number	Genotype	Condition (1)	Tissue with DAF-2 degradation	Mean Lifespan	Median Lifespan	0.95 LCL (2)	0.95 UCL (2)	# deaths/ total	Adjusted p-values using Log-Rank test (3)
1	2 (a)	N2	*wt*	NA	NA	20.2	21	21	22	47/61	NA
	2 (a)	EN462	*kr462 III*	NA	NA	20.9	22	21	22	47/58	vs N2: ns
2	2 (a)	N2	*wt*	NA	NA	20.3	20	20	23	54/80	NA
	2 (a)	EN462	*kr462 III*	NA	NA	19.4	20	17	20	62/80	vs N2: ns
3	2 (b)	N2	*wt*	EtOH	NA	23.1	23	21	27	41/80	NA
	2 (b)	FS428	*daf-2(e1370) III*	EtOH	mutants *e1370*	48.1	50	50	54	65/80	vs N2: ***; vs Ubiquitous 1: ns
	2 (b)	EN7563	*kr462 III; krSi50[Peft-3::TIR1::tagBFP] IV*	EtOH	No degradation - TIR1 Ubiquitous 1	24.8	27	23	27	50/80	vs N2: ns; vs Ubiquitous 1: ***
	2 (b)	EN7563	*kr462 III; krSi50[Peft-3::TIR1::tagBFP] IV*	Aux	Ubiquitous 1	46.6	50	50	50	78/80	vs N2: ***
4	3 (a) - 3 (e) - 3 (h)	N2	*wt*	EtOH	NA	23.4	24	21	24	54/80	NA
	-	EN7563	*kr462 III; krSi50[Peft-3::TIR1::tagBFP] IV*	EtOH	No degradation - TIR1 Ubiquitous 1	26.7	27	24	31	55/82	vs N2: **; vs Ubiquitous 1: ***
	3 (a) - 3 (e) - 3 (h)	EN7563	*kr462 III; krSi50[Peft-3::TIR1::tagBFP] IV*	Aux	Ubiquitous 1	42.3	52	48	52	68/81	vs N2: ***
	3 (a)	EN7565	*kr462 III; krSi55[Pmyo-3::TIR1::tagBFP] V*	Aux	Muscle 1	20.7	21	21	21	53/80	vs N2: **; vs Ubiquitous 1: ***
	3 (h)	EN7567	*kr462 III; krSi36[Prab-3::TIR1::tagBFP] V*	Aux	Neuron 1	32.3	34	31	38	65/80	vs N2: ***; vs Ubiquitous 1: ***
	3 (e)	EN7569	*krSi63[Pdpy-7::TIR1::tagBFP] II; kr462 III*	Aux	Epidermis 1	20.8	21	21	21	58/80	vs N2: ***; vs Ubiquitous 1: ***
	-	EN7691	*ieSi61[Pges-1::TIR1::mRuby + Cbr-unc-119(+)] II; kr462 III*	Aux	Intestine 1	40.7	41	41	41	33/63	vs N2: ***; vs Ubiquitous 1: ***
5	2 (c) - 3 (b) - 3 (d) - 3 (i)	N2	*wt*	EtOH	NA	23	24	21	27	55/78	NA
	2 (c)	FS428	*daf-2(e1370) III*	EtOH	mutants *e1370*	33	42	38	45	54/75	vs N2: ***; vs Ubiquitous 2: ns
	2 (c)	EN7863	*kr462 III; krSi45[Peft-3::TIR1::tagBFP] V*	EtOH	No degradation - TIR1 Ubiquitous 2	23.6	24	24	27	62/80	vs N2: ns; vs Ubiquitous 2: ***
	2 (c) - 3 (b) - 3 (d) - 3 (i)	EN7863	*kr462 III; krSi45[Peft-3::TIR1::tagBFP] V*	Aux	Ubiquitous 2	32.9	45	38	49	66/80	vs N2: ***
	3 (b)	EN7864	*krSi81[Pmyo-3::TIR1::tagBFP] I; kr462 III*	Aux	Muscle 2	23.9	24	21	24	62/81	vs N2: ns; vs Ubiquitous 2: ***
	3 (i)	EN7865	*kr462 III; krSi140[Prab-3::TIR1::tagBFP] IV*	Aux	Neuron 2	32	42	35	42	76/84	vs N2: ***; vs Ubiquitous 2: ***
	3 (d)	EN7862	*ieSi68[Psun-1::TIR1::mRuby::htp-1 3'UTR + Cbr-unc-119(+)] II; kr462 III*	Aux	Germline 2	23.2	24	21	24	65/79	vs N2: ns; vs Ubiquitous 2: ***
6	3 (c) - 3 (g)	EN462	*kr462 III*	EtOH	NA	23.7	25	23	28	63/78	NA
	3 (c) - 3 (g)	EN7863	*kr462 III; krSi45[Peft-3::TIR1::tagBFP] V*	Aux	Ubiquitous 2	29.3	39	30	49	74/76	vs *kr462* : ***
	3 (c)	EN7861	*kr462 III; ieSi38[Psun-1::TIR1::mRuby::sun-1 3'UTR + Cbr-unc-119(+)] IV*	Aux	Germline 1	22.6	23	23	23	79/79	vs *kr462* : ns; vs Ubiquitous 2: ***
	3 (g)	EN7691	*ieSi61[Pges-1::TIR1::mRuby + Cbr-unc-119(+)] II; kr462 III*	Aux	Intestine 1	31.3	35	35	37	67/82	vs *kr462* : ***; vs Ubiquitous 2: ***
7	3 (j)	EN462	*kr462 III*	EtOH	NA	22.2	25	21	25	55/73	NA
	3 (j)	EN7563	*kr462 III; krSi50[Peft-3::TIR1::tagBFP] IV*	Aux	Ubiquitous 1	39	42	42	46	75/87	vs *kr462* : ***
	-	EN7863	*kr462 III; krSi45[Peft-3::TIR1::tagBFP] V*	Aux	Ubiquitous 2	45	53	53	60	60/76	vs *kr462* : ***; vs Ubiquitous 1: ***
	3 (j)	EN7691	*ieSi61[Pges-1::TIR1::mRuby + Cbr-unc-119(+)] II; kr462 III*	Aux	Intestine 1	35.4	35	35	39	62/68	vs *kr462* : ***; vs Ubiquitous 1: ***
	-	EN7567	*kr462 III; krSi36[Prab-3::TIR1::tagBFP] V*	Aux	Neuron 1	27.2	25	25	32	51/56	vs *kr462* : ***; vs Ubiquitous 1: ***
	-	EN7865	*kr462 III; krSi140[Prab-3::TIR1::tagBFP] IV*	Aux	Neuron 2	31.4	32	32	35	59/73	vs *kr462* : ***; vs Ubiquitous 1: ***
	3 (j)	EN7964	*ieSi61[Pges-1::TIR1::mRuby + Cbr-unc-119(+)] II; kr462 III; krSi36[Prab-3::TIR1::tagBFP] V*	Aux	Intestine 1 + Neuron 1	33.2	35	32	35	77/81	vs *kr462:* ***; vs Ubiquitous 1: ***; vs Intestine 1: ns
8	3 (f) - 3 (h)	EN462	*kr462 III*	Aux	NA	23.3	23	23	25	51/78	NA
	3 (f) - 3 (h)	EN7563	*kr462 III; krSi50[Peft-3::TIR1::tagBFP] IV*	Aux	Ubiquitous 1	42.4	49	46	49	68/80	vs *kr462* : ***
	-	EN7567	*kr462 III; krSi36[Prab-3::TIR1::tagBFP] V*	Aux	Neuron 1	33.6	37	35	37	70/80	vs *kr462* : ***; vs Ubiquitous 1: ***
	-	EN7691	*ieSi61[Pges-1::TIR1::mRuby + Cbr-unc-119(+)] II; kr462 III*	Aux	Intestine 1	33.4	35	32	37	52/73	vs *kr462* : ***; vs Ubiquitous 1: ***
	-	EN7964	*ieSi61[Pges-1::TIR1::mRuby + Cbr-unc-119(+)] II; kr462 III; krSi36[Prab-3::TIR1::tagBFP] V*	Aux	Intestine 1 + Neuron 1	35.1	37	32	39	69/80	vs *kr462* : ***; vs Ubiquitous 1: ***; vs Neuron 1: ns
	3 (f)	EN8032	*kr462 III; krSi53[Pdpy-7::TIR1::tagBFP] III*	Aux	Epidermis 2	25.8	25	25	28	49/78	vs *kr462* : ***; vs Ubiquitous 1: ***
	3 (h)	EN8173	*reSi5[Pges-1::TIR1::F2A::mTagBFP2::NLS::AID::tbb-2 3'UTR] I; kr462 III*	Aux	Intestine 2	37.2	42	37	44	43/79	vs *kr462* : ***; vs Ubiquitous 1: ***

(1) EtOH: ethanol; Aux: 1 mM Auxine; PQ: 20 mM paraquat

(2) LCL: Lower Confidence Limit; UCL: Upper Confidence Limit

(3) Comparisons between strains in the same experiment (see first column, "experiment number")

Adjusted p-value: ns: not significant; * < 0.05; ** < 0.01; *** < 0.001

Table S2: Lifespan measurements

Experiment number	Corresponding Figure	Strain number	Genotype	Condition (1)	Tissue with DAF-2 degradation	Mean Lifespan	Median Lifespan	0.95 LCL (2)	0.95 UCL (2)	# deaths/ total	Adjusted p-values using Log-Rank test (3)
9	3 (l)	EN462	*kr462 III*	Aux + PQ	NA	2.6	2.6	2.6	2.6	53/75	NA
	3 (l)	EN7563	*kr462 III; krSi50[Peft-3::TIR1::tagBFP] IV*	Aux + PQ	Ubiquitous 1	3.9	4.7	4.7	6	69/75	vs *kr462* : ***
	3 (l)	EN7863	*kr462 III; krSi45[Peft-3::TIR1::tagBFP] V*	Aux + PQ	Ubiquitous 2	3.9	6	6	6	73/75	vs *kr462* : ***; vs Ubiquitous 1: ***
	3 (l)	EN7691	*ieSi61[Pges-1::TIR1::mRuby + Cbr-unc-119(+)] II; kr462 III*	Aux + PQ	Intestine 1	3.5	3.6	3.6	3.6	67/75	vs *kr462* : ***; vs Ubiquitous 1: ***
	3 (l)	EN8173	*reSi5[Pges-1::TIR1::F2A::mTagBFP2::NLS::AID::tbb-2 3'UTR] I; kr462 III*	Aux + PQ	Intestine 2	3.2	3	3	3.6	71/75	vs *kr462* : ***; vs Ubiquitous 1: ***
10	3 (m) - Sup 2	EN462	*kr462 III*	Aux + PQ	NA	2.6	2.6	2.6	2.6	84/100	NA
	3 (m) - Sup 2	EN7563	*kr462 III; krSi50[Peft-3::TIR1::tagBFP] IV*	Aux + PQ	Ubiquitous 1	3.9	4.2	4.2	4.8	81/100	vs *kr462* : ***
	Sup 2	EN7863	*kr462 III ;krSi45[Peft-3::TIR1::tagBFP] V*	Aux + PQ	Ubiquitous 2	4.2	5.6	5.6	6.8	78/100	vs *kr462* : ***; vs Ubiquitous 1: ***
	Sup 2	EN7565	*kr462 III; krSi55[Pmyo-3::TIR1::tagBFP] V*	Aux + PQ	Muscle 1	2.6	2.6	2.6	2.6	92/99	vs *kr462* : ns; vs Ubiquitous 1: ***
	Sup 2	EN7864	*kr462 III; krSi81[Pmyo-3::TIR1::tagBFP] I*	Aux + PQ	Muscle 2	2.6	2.6	2.6	2.6	97/100	vs *kr462* : ns; vs Ubiquitous 1: ***
	3 (m)	EN7567	*kr462 III; krSi36[Prab-3::TIR1::tagBFP] V*	Aux + PQ	Neuron 1	2.2	2	2	2	95/100	vs *kr462* : ***; vs Ubiquitous 1: ***
	3 (m)	EN7865	*kr462 III; krSi140[Prab-3::TIR1::tagBFP] IV*	Aux + PQ	Neuron 2	2.9	2.6	2.6	3	89/97	vs *kr462* : ***; vs Ubiquitous 1: ***
	-	EN7691	*ieSi61[Pges-1::TIR1::mRuby + Cbr-unc-119(+)] II; kr462 III*	Aux + PQ	Intestine 1	3.5	3.6	3.6	3.6	96/100	vs *kr462* : ***; vs Ubiquitous 1: ***
11	3 (n)	EN462	*kr462 III*	Aux + PQ	NA	2.8	3	2.5	3	74/91	NA
	3 (n)	EN7563	*kr462 III; krSi50[Peft-3::TIR1::tagBFP] IV*	Aux + PQ	Ubiquitous 1	4.4	5	5	5.5	73/90	vs *kr462* : ***
	-	EN7565	*kr462 III; krSi55[Pmyo-3::TIR1::tagBFP] V*	Aux + PQ	Muscle 1	2.7	2.5	2.5	3	63/92	vs *kr462* : *; vs Ubiquitous 1: ***
	3 (n)	EN7567	*kr462 III; krSi36[Prab-3::TIR1::tagBFP] V*	Aux + PQ	Neuron 1	2.3	2.5	2.5	2.5	75/90	vs *kr462* : ***; vs Ubiquitous 1: ***
	-	EN7865	*kr462 III; krSi140[Prab-3::TIR1::tagBFP] IV*	Aux + PQ	Neuron 2	3.2	3	2.5	3	49/92	vs *kr462* : **; vs Ubiquitous 1: ***
	3 (n)	EN7691	*ieSi61[Pges-1::TIR1::mRuby + Cbr-unc-119(+)] II; kr462 III*	Aux + PQ	Intestine 1	3.7	3.5	3.5	3.5	72/92	vs *kr462* : ***; vs Ubiquitous 1: ***
	3 (n)	EN7964	*ieSi61[Pges-1::TIR1::mRuby + Cbr-unc-119(+)] II; kr462 III; krSi36[Prab-3::TIR1::tagBFP] V*	Aux + PQ	Intestine 1 + Neuron 1	3.1	3	3	3.5	71/91	vs *kr462* : ***; vs Ubiquitous 1: ***; vs Intestine 1: ***

(1) EtOH: ethanol; Aux: 1 mM Auxine; PQ: 20 mM paraquat

(2) LCL: Lower Confidence Limit; UCL: Upper Confidence Limit

(3) Comparisons between strains in the same experiment (see first column, "experiment number")

Adjusted p-value: ns: not significant; * < 0.05; ** < 0.01; *** < 0.001

Table S3: dauer percentage

	Percentage of dauer (n; N)	
TIR1 strain (see Table S1)	**+ EtOH**	**+ Auxin**
Ubiquitous 1	0 (1640; 5)	100 (605; 5)
Ubiquitous 2	0 (112; 3)	100 (68; 3)
Neuron 1	0 (761; 3)	0 (546; 3)
Neuron 2	0 (164; 3)	0 (157; 3)
Muscle 1	0 (626; 3)	0 (633; 3)
Intestine 1	0 (1153; 4)	0 (984; 4)
Epidermis 1	0 (670; 2)	0 (421; 2)
Germline 2	0 (189; 3)	0 (143; 3)
Neuron 1 + Muscle 1	0 (427; 2)	0 (366; 2)
Neuron 1 + Intestine 1	0 (201; 3)	0 (170; 3)

Table S4: DAF-16 nuclear translocation

		Percentage of worms with strong DAF-16::wSCARLET nuclear signal (n)		
		Intestine	Neurons	Muscles
DAF-2 degradation	Control	0 (22)	0 (25)	0 (22)
	Ubiquitous	100 (31)	100 (28)	100 (32)
	Intestine	100 (21)	0 (21)	100 (22)
	Neuron	0 (25)	100 (28)	0 (25)
	Muscle	0 (25)	0 (25)	100 (25)

Table S5

List of generated plasmids

Plasmid	Description	Usage
pCR12	*last 280 bp of daf-2::flexible linker::AID::flexible linker::mNeonGreen::daf-2 3'UTR first 347 bp*	Repair template to create EN462 CRISPR knock-in strain
pCV06	*Punc-17::TIR1-TagBFP::unc-54 3'UTR*	insertion; used to create *krSi52* allele; contains a neomycin-resistant cassette
pCV07	*Punc-47::TIR1-TagBFP::unc-54 3'UTR*	insertion; used to create *krSi51* allele; contains a neomycin-resistant cassette
pBB16	*Pmyo-3::tom-20N::wScarlet::unc-54 3'UTR*	*20N::wSCARLET* insertion; used to create *krSi134* allele; contains a neomycin-resistant cassette

List of miniMos single-copy insertion alleles

Allele name	Construct	Plasmid used
krSi45	*Peft-3::TIR1::tagBFP V*	pCV09 (Zhou et al., 2021)
krSi81	*Pmyo-3::TIR1::tagBFP I*	pCV04 (Zhou et al., 2021)
krSi140	*Prab-3::TIR1::tagBFP IV*	pCV05 (Zhou et al., 2021)
krSi53	*Pdpy-7::TIR1::tagBFP III*	pCV08 (Zhou et al., 2021)
krSi51	*Punc-47::TIR1::BFP IV*	pCV07 (this work)
krSi52	*Punc-17::TIR1::BFP*	pCV06 (this work)
krSi134	*Pmyo-3::tom-20N::wScarlet I*	pBB16 (this work)